PDRMIP: A precipitation driver and response model intercomparison project—Protocol and preliminary results

Gunnar Myhre, Piers M. Forster, Bjørn H. Samset, Øivind Hodnebrog, Jana Sillmann, S. G. Aalbergsjø, Timothy Andrews, Olivier Boucher, Gregory Faluvegi, D. Fläschner, T. Iversen, Matthew M. Kasoar, Viatcheslav V. Kharin, Alf Kirkevåg, Jean-Francois Lamarque, Dirk Olivié, Thomas B. Richardson, Drew Shindell, Keith P. Shine, Camilla W. Stjern, Toshihiko Takemura, Apostolos Voulgarakis & Francis Zwiers

2017

Pacific Climate Impacts Consortium (PCIC)

PCIC Publications

Original citation:

Myhre, G., Forster, P. M., Samset, B. H., Hodnebrog, Ø., Sillmann, J., Aalbergsjø, S. G., Andrews, T., Boucher, O., Faluvegi, G., Fläschner, D., Iversen, T., Kasoar, M., Kharin, V. V., Kirkevåg, A., Lamarque, J.-F., Olivié, D., Richardson, T. B., Shindell, D., Shine, K. P., … Zwiers, F. W. (2017). PDRMIP: A precipitation driver and response model intercomparison project—Protocol and preliminary results. *Bulletin of the American Meteorological Society, 98*(6), 1185–1198. https://doi.org/10.1175/BAMS-D-16-0019.1

PDRMIP

A Precipitation Driver and Response Model Intercomparison Project—Protocol and Preliminary Results

G. Myhre, P. M. Forster, B. H. Samset, Ø. Hodnebrog, J. Sillmann, S. G. Aalbergsjø, T. Andrews, O. Boucher, G. Faluvegi, D. Fläschner, T. Iversen, M. Kasoar, V. Kharin, A. Kirkevåg, J.-F. Lamarque, D. Olivié, T. B. Richardson, D. Shindell, K. P. Shine, C. W. Stjern, T. Takemura, A. Voulgarakis, and F. Zwiers

PDRMIP investigates the role of various drivers of climate change for mean and extreme precipitation changes based on multiple climate model output and energy budget analyses.

Changes to both mean and extreme precipitation have been observed over the last century, due partly to global warming, and changes are expected to become more marked during the course of this century (IPCC 2013). Human society is vulnerable to changes in precipitation, because of the importance of precipitation for freshwater availability and food production, but also because of potential damages to infrastructure caused by extreme precipitation.

Robust changes in regional precipitation patterns have been found across current climate models from phase 5 of the Coupled Model Intercomparison Project (CMIP5) for the industrial era and future climate, such as a drying in many subtropical regions and enhanced precipitation at high latitudes. However, the diversity among the CMIP5 models is large both in terms of global-mean and regional predicted precipitation change (Knutti and Sedláček 2013). Furthermore, evaluation of the current generation of climate models reveals precipitation biases (Flato et al. 2013; Mehran et al. 2014). Extensive studies have been performed on how precipitation responds to climate change using observations and

AFFILIATIONS: Myhre, Samset, Hodnebrog, Sillmann, Aalbergsjø, and Stjern—Center for International Climate and Environmental Research—Oslo, Oslo, Norway; Forster and Richardson—University of Leeds, Leeds, United Kingdom; Andrews—Met Office Hadley Centre, Exeter, United Kingdom; Boucher—Laboratoire de Météorologie Dynamique, Institut Pierre Simon LaPlace, Université Pierre-et-Marie-Curie Centre National de la Recherche Scientifique, Paris, France; Faluvegi—Columbia University, New York, New York; Fläschner—Max-Planck-Institut für Meteorologie, Hamburg, Germany; Iversen, Kirkevåg, and Olivié—Norwegian Meteorological Institute, Oslo, Norway; Kasoar and Voulgarakis—Imperial College London, London, United Kingdom; Kharin—Canadian Centre for Climate Modelling and Analysis, Victoria, British Columbia, Canada; Lamarque—National Center for Atmospheric Research, Boulder, Colorado; Shindell—Duke University, Durham, North Carolina; Shine—University of Reading, Reading, United Kingdom; Takemura—Kyushu University, Fukuoka, Japan; Zwiers—Pacific Climate Impacts Consortium, University of Victoria, Victoria, British Columbia, Canada
CORRESPONDING AUTHOR: G. Myhre, gunnar.myhre@cicero.oslo.no

The abstract for this article can be found in this issue, following the table of contents.
DOI:10.1175/BAMS-D-16-0019.1

In final form 29 September 2016

modeling (e.g., Trenberth 2011), but significant questions still remain, particularly with respect to dynamical changes on precipitation (Muller and O'Gorman 2011).

The precipitation at a particular location is highly variable and depends on local and actual weather conditions. However, on a global scale, precipitation is strongly constrained by the energy budget within the climate system (Mitchell et al. 1987; Allen and Ingram 2002; Stephens et al. 2012) and is described in more detail in the sidebar on precipitation changes and the energy budget.

The energy budget is altered by both natural and anthropogenic influences. Depending on the physical properties of a climate forcing mechanism, it causes either a fast response in precipitation on time scales from days to weeks or a slower response on a time scale of years (Andrews et al. 2010; Ming et al. 2010; Frieler et al. 2011; Pendergrass and Hartmann 2012), or both (see Fig. SB1). Bala et al. (2010) suggested that multimodel comparisons should be constructed such that fast and slow precipitation responses could be separately evaluated. It has been shown in several model studies that the global-mean fast atmospheric response correlates strongly with the atmospheric component of radiative forcing, while the slower response scales with global surface temperature change (Andrews et al. 2010; Kvalevåg et al. 2013), which has a long time scale because of the large thermal capacity of the ocean. Figure 1 illustrates these fast and slow precipitation changes for various drivers of climate change from two climate models (Andrews et al. 2010; Kvalevåg et al. 2013) combined with the new Precipitation Driver and Response Model Intercomparison Project (PDRMIP) results (Samset et al. 2016).

On regional scales the fast precipitation response is more complex because of changes in atmospheric circulation. Rapid circulation changes in response to forcing are associated with the change in atmospheric absorption (Bony et al. 2013; Merlis 2015), as well as the rapid land surface response (Shaw and Voigt 2015; Richardson et al. 2016). The land surface temperature responds on very short time scales and can drive significant shifts in tropical convection and precipitation (Dong et al. 2014). As a result, climate drivers such as sulfate aerosols or changes in the solar constant, which have small effects on atmospheric absorption, can still produce rapid spatial shifts in precipitation as a result of the surface forcing. Heterogeneity of radiative forcings [e.g., sulfate and black carbon (BC)] will also lead to distinct regional precipitation responses through changes in atmospheric circulation. Further descriptions of rapid adjustments, which include the fast precipitation changes caused by atmospheric absorption, are discussed by Boucher et al. (2013), Myhre et al. (2013a), and Sherwood et al. (2015).

The drivers of climate change included in Fig. 1 span a wide range of agents for atmospheric absorption, causing different rapid adjustments as well as slower responses from surface temperature change. Ming et al. (2010) and Kvalevåg et al. (2013) found a strong dependence of the fast response on the location of BC concentration with height. For ozone forcing changes, Andrews et al. (2010) found both fast and slow precipitation responses to be small, but

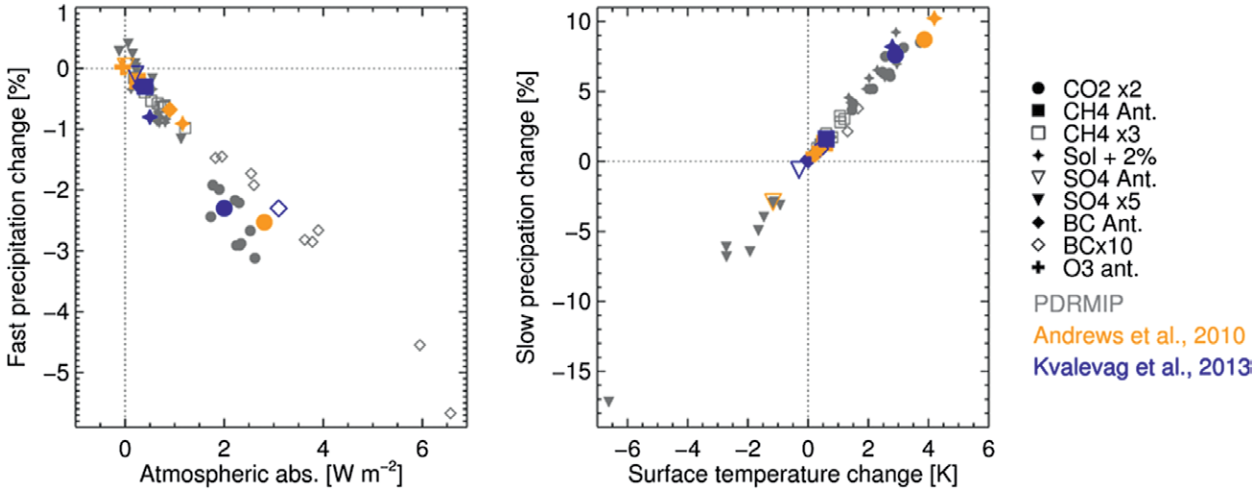

Fig. 1. (left) Fast and (right) slow global precipitation responses as functions of atmospheric absorption and surface temperature change from two modeling studies (Andrews et al. 2010; Kvalevåg et al. 2013) combined with PDRMIP results from Samset et al. (2016), as well as PDRMIP results from the IPSL-CM5A model. "Ant" in the legend denotes anthropogenic changes.

The latent heat flux from evaporation and transpiration of water at the surface is compensated through the net condensation flux in the atmosphere. The global energy budget (at the top of the atmosphere, in the atmosphere, and at the surface) is nearly in balance. Hence, the effect of a change in atmospheric composition on the energy budget is a useful framework for understanding the resulting changes in precipitation. In Fig. SB1, we break down the responses schematically, for three time scales: i) A perturbation may initially alter precipitation as a result of changes in the atmospheric radiative heating or cooling, which depends mainly on the radiative forcing agent. The change in atmospheric radiative cooling occurs more or less instantaneously. ii) Next, atmospheric temperature, clouds, and water vapor are modified as a result of the changes in atmospheric radiative heating or cooling. These so-called rapid adjustments further alter precipitation. iii) Finally, precipitation is affected through climate feedback processes in response to the subsequent surface temperature changes, on time scales from years to decades.

Higher temperatures lead to increased atmospheric water vapor concentrations. Theoretical and model studies show that the global-mean precipitation increases with global temperature change across a range from 1% to 3% K^{-1} (O'Gorman et al. 2012; Collins et al. 2013). Because of energetic constraints, this is considerably smaller than the increase in vapor pressure, with temperature (6%–7% K^{-1}) (Mitchell et al. 1987; Allen and Ingram 2002; O'Gorman et al. 2012; Allan et al. 2014; Pendergrass and Hartmann 2014). As shown in Fig. SB1, and introduced earlier, the energy budget of the troposphere must be approximately balanced. To first order, the global-mean atmospheric radiative cooling is balanced by latent heating through condensation and freezing minus the reevaporation of precipitation and sensible heat. Changes in atmospheric radiative cooling (due to the forcing agent itself or as a result of climate feedbacks) will therefore impact the release of latent heat and precipitation (Allen and Ingram 2002). This explains why the global-mean precipitation changes do not simply scale with the amount of available water. Increased surface temperature and a constant lapse rate enhance the atmospheric radiative cooling. For most drivers of climate change, this is the dominant factor for precipitation changes (Andrews et al. 2010; Boucher et al. 2013; Samset et al. 2016). However, for the major driver of climate change, CO_2, the rapid adjustments cause a precipitation decrease that can significantly offset the increase driven by surface temperature increases.

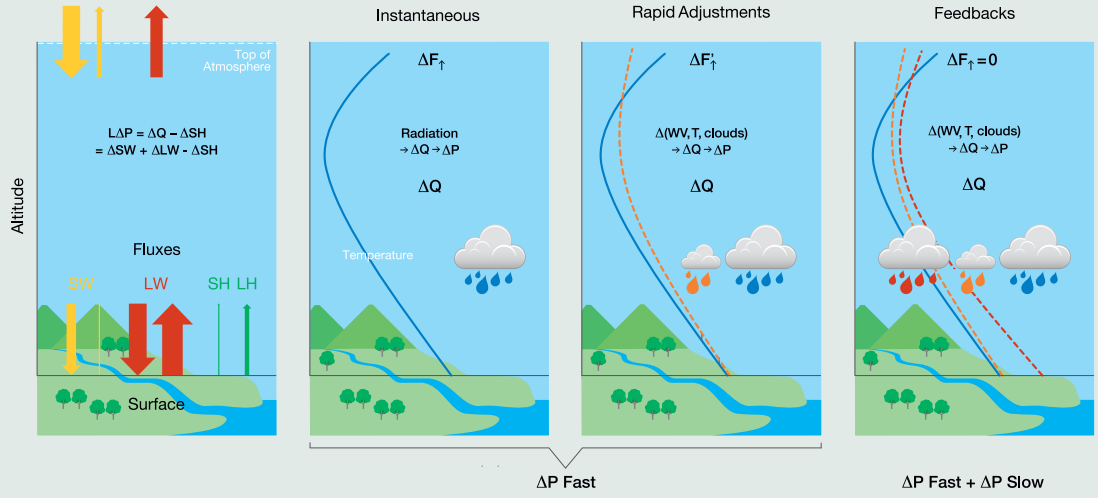

FIG. SB1. Schematic diagram of the energy fluxes and fast and slow precipitation change (Δ*P*) processes. (left) At the TOA, in the atmosphere, and at the surface, the energy budget is nearly in balance on a global scale. Changes in the atmospheric radiative cooling Δ*Q* can be caused by changes in absorption of shortwave radiation (SW) or changes in absorption/emission of longwave radiation (LW) or both. Here, LH = *L*Δ*P* is the latent heat and SH is the sensible heat. (left center) An external driver of climate change alters the radiative fluxes at the top of the atmosphere and this may alter the atmospheric absorption. (right center) The instantaneous change through radiation may further alter the atmospheric temperature, water vapor, and clouds, through rapid adjustments. These rapid adjustments may lead to decreases or increases in clouds and water vapor, and they can vary through the atmosphere. The instantaneous radiative perturbation and rapid adjustments change precipitation on a fast time scale (from days to a few years). (right) Climate feedback processes through changes in the surface temperature further alter the atmospheric absorption, which occurs on a long time scale (decades). Net radiative fluxes at the TOA are given as *F*, water vapor as WV, temperature as *T*, and latent heat of vaporization as *L*. In the left center and right panels, the blue curve indicates the unperturbed state, the orange curve represents the rapid adjustments, and the red curve represents the effects of both fast and slow adjustments.

recently MacIntosh et al. (2016) found that for the industrial era, the fast precipitation response from ozone changes is also strongly dependent on the altitude of the ozone change. Stratospheric aerosols are also found to yield a fast precipitation response (Ferraro and Griffiths 2016). Fläschner et al. (2016) showed that accounting for differences in the fast precipitation response explains much of the previously reported large variation in hydrological sensitivity (change in global-mean precipitation per global-mean temperature change) between climate models. The estimated factor-of-3 spread in the hydrological sensitivity (Held and Soden 2006; Previdi 2010; Pendergrass and Hartmann 2014) can be reduced to an intermodel spread of 1.5 when a correction is made for the diversity in rapid adjustment (Fläschner et al. 2016). An additional source of spread in hydrological sensitivity has been identified as intermodel differences in the representation of absorption of shortwave radiation relating to the representation of radiative transfer by water vapor (e.g., Takahashi 2009; DeAngelis et al. 2015; Fildier and Collins 2015). This enhanced atmospheric absorption, as water vapor concentrations increase, is conceptually similar to the drivers of fast precipitation change, but since the water vapor change is driven by feedbacks on the global energy budget, it is better viewed as part of the slow response.

The rates of extreme precipitation events have been found, through both observations and modeling, to scale closely with the Clausius–Clapeyron relationship rather than with global-mean precipitation change (Allan and Soden 2008; Boucher et al. 2013; O'Gorman 2015). This is supported by several CMIP5 studies (e.g., Kharin et al. 2013; Sillmann et al. 2013a; Pendergrass et al. 2015), which indicate that increases in globally averaged extreme precipitation are about 3 times as large as the increase in mean precipitation under different greenhouse gas emission scenarios. The scaling of extreme precipitation with temperature may however be much more complex than what is implied by the Clausius–Clapeyron relationship, with considerable regional variations due to various dynamic and thermodynamic mechanisms (e.g., Caesar and Lowe 2012; Westra et al. 2013). From the CMIP5 ensemble, the increase in 20-yr return values of the annual extremes of daily precipitation is estimated to be about 6% K^{-1}, with a large intermodel range between 4% and 10% K^{-1} according to Kharin et al. (2013). This considerable uncertainty in estimates of the Clausius–Clapeyron relationship for extreme precipitation compared to mean precipitation is most pronounced in the tropics. The physical understanding of this larger increase in extreme precipitation per global temperature change is based on the fact that relative humidity is expected, from both observations and climate models, to be approximately constant in a warmer climate. Water vapor content in the lower atmosphere will therefore increase by 6%–7% K^{-1} of warming, thus making more water available for intense precipitation events. Furthermore, there are indications from both observations and modeling studies that subdaily (or hourly) extreme precipitation may increase even faster than suggested by the Clausius–Clapeyron relationship (Lenderink and Van Meijgaard 2008; Berg et al. 2013; Kendon et al. 2014; Westra et al. 2014). However, this has recently been questioned and could be related to sampling issues (Ban et al. 2015). Recent findings nonetheless indicate that changes in the storm dynamics may result in precipitation changes that are greater than those implied by the Clausius–Clapeyron relationship (Wasko et al. 2016). Different drivers of climate change may impact the extreme precipitation differently and Sillmann et al. (2013b) found a relatively large impact of aerosol reductions on climate extremes over Europe in a climate model.

The range in atmospheric absorption associated with the drivers of climate change is important for understanding precipitation changes and the associated model diversity, as illustrated in Fig. 1. However, no dedicated model intercomparison project has previously been undertaken, leaving open the question of whether rapid adjustments are indeed similarly represented across models with respect to precipitation changes. We thus present here PDRMIP (www.cicero.uio.no/en/PDRMIP), an open international study designed to extend the analysis of the impacts of single precipitation drivers, on short and long time scales, to a broad range of climate models. The aim of PDRMIP is to perform a thorough investigation of the differences in the effects of anthropogenic and natural drivers on precipitation and extreme precipitation events. This will be accomplished based on five core simulations, with global perturbation to either anthropogenic or natural drivers of climate change, as well as six selected regional perturbation experiments.

PDRMIP will in particular enhance our understanding of drivers of climate change other than CO_2 on cloud changes, climate sensitivity, and precipitation, including extremes. At present a wide range of forcing mechanisms contribute to climate change (Forster et al. 2007; Myhre et al. 2013a). The efficacy of different drivers of climate change to change the surface temperature from a radiative

forcing perturbation has been compared to CO_2 in individual models (Hansen et al. 2005; Yoshimori and Broccoli 2008); in PDRMIP, this will be performed with a large set of climate models. The focus is on the global climate perspective, with additional work examining changes in precipitation over land versus ocean, and over key regions of the globe. Since most of the analysis of PDRMIP has been performed ahead of completion of the ongoing CMIP6 exercise, the results will greatly contribute to understanding aspects of the CMIP6 results.

EXPERIMENTAL DESIGN. PDRMIP asks modeling groups to perform one baseline and five core perturbation experiments, complemented by up to six regional simulations, in order to explore the responses to climate drivers occurring in different regions, which have been suggested to vary strongly (Shindell et al. 2012). The core experiments consist of simulations with a doubling of CO_2 concentration, tripling of CH_4 concentration, a 2% increase in total solar irradiance, and two experiments increasing the anthropogenic aerosol concentrations (see Table 1). The additional simulations are dedicated to regional changes in aerosols and ozone, the climate drivers that feature strong spatial variability (see Table 2). These simulations are related to the large increase in aerosols and their precursors over Southeast Asia over the past few decades and potential mitigation efforts.

For models where it is possible to prescribe aerosol concentration fields, PDRMIP provides a common set of baseline and perturbed concentrations. This is done in order to minimize the effect on the results from differences in geographical and vertical aerosol distributions in the models. It is known that despite identical aerosol fields, the forcing will differ as a result of varying complexities in aerosol–radiation and aerosol–cloud interactions, as well as host model differences (Stier et al. 2013). This is therefore also likely a cause for intermodel variability in precipitation change estimates. The baseline PDRMIP aerosol fields are constructed from the multimodel mean from phase 2 of the Aerosol Comparisons between Observations and Models (AeroCom) science initiative (see Fig. 2). Models that are only able to drive aerosol fields through emissions will instead scale their native emission fields. Even though this introduces additional variability into the results, it is highly preferable to still have these models participate. We note that rapid adjustments associated with climate drivers with significant change in atmospheric radiative cooling, especially CO_2 and black carbon (Boucher et al. 2013; Myhre et al. 2013a; Sherwood et al. 2015), are unavoidably included in

Table 1. PDRMIP core experiments. All experiments are performed with both fixed-SST (a minimum of 15 yr) and coupled model configurations (100 yr).

Name	Description
Base	Specified all anthropogenic and natural climate forcing agents at present-day abundances (preferred) or preindustrial abundances
CO_2 × 2	Doubling of the CO_2 concentration relative to base
CH_4 × 3	Tripling of the CH_4 concentration relative to base
Solar + 2%	Total solar irradiance is increased by 2%
Sul × 5	Increase in the anthropogenic sulfate concentration or emissions by 5 times relative to base
BC × 10	Increase in the anthropogenic BC concentration or emissions by 10 times relative to base

Table 2. PDRMIP additional experiments. All experiments are performed with both fixed-SST and coupled model configurations. The European region is defined as 35°–70°N, 10°W–40°E. Likewise, the region of Asia is defined as 10°–50°N, 60°–140°E.

Name	Description
Sulred	Sulfate concentration from present-day concentrations to preindustrial concentrations
Suleur	Sulfate present-day anthropogenic concentration multiplied by 10, for Europe only
Sulasia	Sulfate present-day anthropogenic concentration multiplied by 10, for Asia only
BCasia	BC present-day anthropogenic concentration multiplied by 10, for Asia only
Sulasiared	Similar to Sulred, but for Asia only
O3asia	Increase in ozone, for Asia only, with comparable forcing to Sulasia

the climate model simulations, and the semidirect cloud effect of black carbon is therefore automatically included in all PDRMIP simulations.

To diagnose both the fast and slow responses in precipitation (Andrews et al. 2010; Bala et al. 2010), the model simulations are performed with both fixed sea surface temperatures (SSTs) and fully coupled (or slab ocean) configurations of the models. The length of the fixed-SST simulations is a minimum of 15 yr and the fully coupled climate simulations are 100 yr long. The fast response is derived from the last 10 yr of the fixed-SST simulations, and the total response from the last 50 yr of the coupled simulations. The slow response is calculated as the fast response subtracted from the total response. The forcing of the climate drivers can be derived from the fixed-SST top-of-the-atmosphere (TOA) fluxes and from the regression of the imbalance in the TOA net radiative fluxes and surface temperature from the coupled simulations (Gregory et al. 2004; Boucher et al. 2013; Myhre et al. 2013a). Additional simulations will be performed by a subset of models to investigate the behavior of the system beyond 100 yr.

PDRMIP model output is in the standardized format from a subset of the CMIP5 output protocol and will be made available to the research community upon request, through a Norwegian national data storage facility.

The list of 10 PDRMIP models (see Table 3 for full model names and descriptions) includes models that either have been used in CMIP5 or will be used in CMIP6. Some of the 10 PDRMIP models are different versions of the same climate models, whereas others are largely independent (Knutti et al. 2013).

GENERAL PDRMIP RESULTS. Figures 1, 3, 4, and 5 show some overall results from the main PDRMIP simulations. Figure 3 shows zonal-mean temperature changes, precipitation changes, radiative forcing, and atmospheric absorption for the five PDRMIP climate drivers. The well-known strong high-latitude temperature response, especially in the Northern Hemisphere, is evident for all five PDRMIP drivers. This is also the case for CH_4 and BC, with smaller temperature responses than for the other drivers. In relative terms, the precipitation changes are largest at high northern latitudes. However, the tropics have greater absolute precipitation and quite large relative changes are found here, but these changes vary with latitude. Changes in precipitation in the subtropics are relatively small for the PDRMIP drivers.

The zonal-mean radiative forcing and atmospheric absorption show that the PDRMIP drivers differ substantially. Of the two drivers mostly affecting longwave radiation, CO_2 has slightly stronger atmospheric absorption than CH_4 when compared to top-of-the-atmosphere radiative forcing (Samset et al. 2016). The atmospheric absorption in the solar and sulfate experiments is weak (also shown in Fig. 1). The corresponding radiative forcings, on the other hand, differ, with strong forcings in the tropics and the largest difference between the tropics and high latitudes in the solar experiment, whereas in the sulfate experiment the forcing has a maximum in absolute terms around 40°N. In the BC experiment the radiative forcing is relatively weak, but with a very strong atmospheric absorption locally reaching more than 8 W m^{-2} in the zonal average.

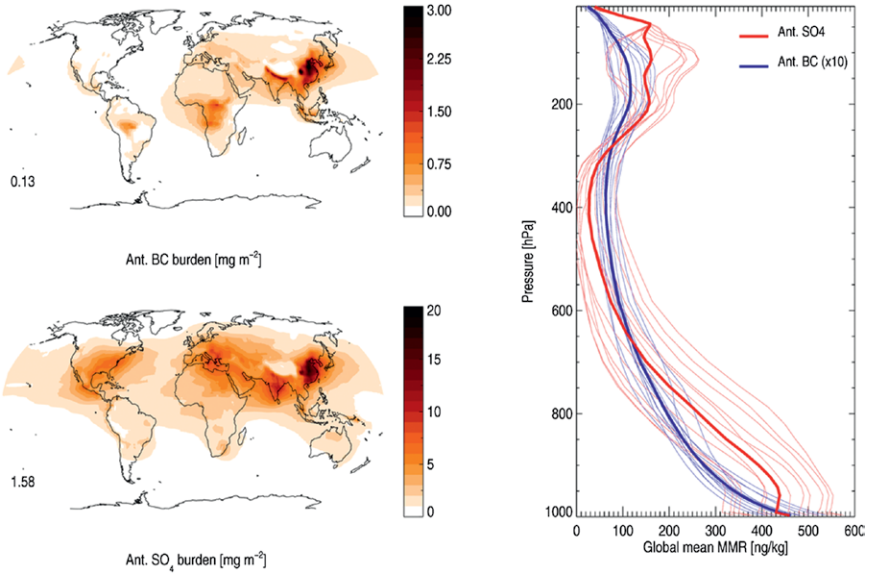

FIG. 2. PDRMIP-prescribed anthropogenic burden and aerosol mass mixing ratio (MMR) fields, constructed from AeroCom, phase II, models (Myhre et al. 2013b). (left) The geographical distribution of the annual-mean burden for (top) BC and (bottom) SO_4 and (right) the vertical profile of MMR, of the present-day increase in aerosol levels due to anthropogenic emissions. Thick lines show the annual means, while thin lines show individual months for the vertical profiles. Note that BC MMR has been scaled by 10 times for clarity.

Table 3. Description of the ten PDRMIP models. GA = Global Atmosphere. HTAP2 = Hemispheric Transport Air Pollution, phase 2.

Model	Version	Resolution	Ocean setup	Aerosol setup	Key references
Second Generation Canadian Earth System Model (CanESM2)	2010	2.8°×2.8°, 35 levels	Coupled ocean	Emissions	Arora et al. (2011)
Community Earth System Model, version 1 (Community Atmosphere Model, version 4) [CESM1(CAM4)]	1.0.3	2.5°×1.9°, 26 levels	Slab ocean	Fixed concentrations	Neale et al. (2010); Gent et al. (2011)
CESM1(CAM5)	1.1.2	2.5°×1.9°, 30 levels	Coupled ocean	Emissions	Hurrell et al. (2013); this is the same model as Kay et al. (2015), but with a coarser resolution; Otto-Bliesner et al. (2016)
Goddard Institute for Space Studies Model E2, coupled with the Russell ocean model (GISS-E2-R)	E2-R	2°×2.5°, 40 levels	Coupled ocean	Fixed concentrations	Schmidt et al. (2014)
Hadley Centre Global Environment Model, version 2—Earth System (includes Carbon Cycle configuration with chemistry) (HadGEM2-ES)	6.6.3	1.875°×1.25°, 38 levels	Coupled ocean	Emissions	Collins et al. (2011); Martin et al. (2011)
HadGEM3	GA 4.0	1.875°×1.25°, 85 levels	Coupled ocean	Fixed concentrations	Bellouin et al. (2011); Walters et al. 2014)
L'Institut Pierre-Simon Laplace Coupled Model, version 5A (IPSL-CM5A)	CMIP5	3.75° × 1.875°, 39 levels	Coupled ocean	Fixed concentrations	Dufresne et al. (2013)
Max Planck Institute Earth System Model (MPI-ESM)	1.1.00p2	T63, 47 levels	Coupled ocean	Climatology, year 2000	Roeckner et al. (2016, unpublished manuscript)
Norwegian Earth System Model, version 1 (NorESM1)	NorESM1-M (intermediate resolution)	2.5°×1.9°, 26 levels	Coupled ocean	Fixed concentrations	Bentsen et al. (2013); Iversen et al. (2013); Kirkevåg et al. (2013)
Model for Interdisciplinary Research on Climate-Spectral Radiation-Transport Model for Aerosol Species (MIROC-SPRINTARS)	5.9.0	T85 (approx 1.4°×1.4°), 40 levels	Coupled ocean	HTAP2 emissions	Takemura et al. (2005); Takemura et al. (2009); Watanabe et al. (2010)

Figure 4 shows the geographical distribution of the multimodel-mean apparent hydrological sensitivity (HS) for the five core PDRMIP climate drivers ($CO_2 \times 2$, $CH_4 \times 3$, solar + 2%, BC × 10, $SO_4 \times 5$). The apparent HS parameter is calculated as the annual-mean geographical precipitation change over the last 50 yr of the PDRMIP coupled/slab-ocean simulations, divided by global- and annual-mean temperature changes relative to the base simulation. The apparent HS includes both the rapid adjustments to the introduction of a climate driver and the resulting slow, purely temperature-driven response. For the three first drivers—CO_2, CH_4, and solar irradiance—differences in the geographical distribution among the drivers are modest. We find weak or negative sensitivities in subtropical regions and strongly positive sensitivities in tropical regions associated with a strengthened ITCZ, as well as at midlatitudes.

The apparent HS from an increase in BC differs substantially from that of the other drivers, especially in the subtropical regions, with smaller differences around the ITCZ and mid- to high latitudes. Unlike the other climate drivers investigated in PDRMIP, the reduced precipitation in subtropical regions

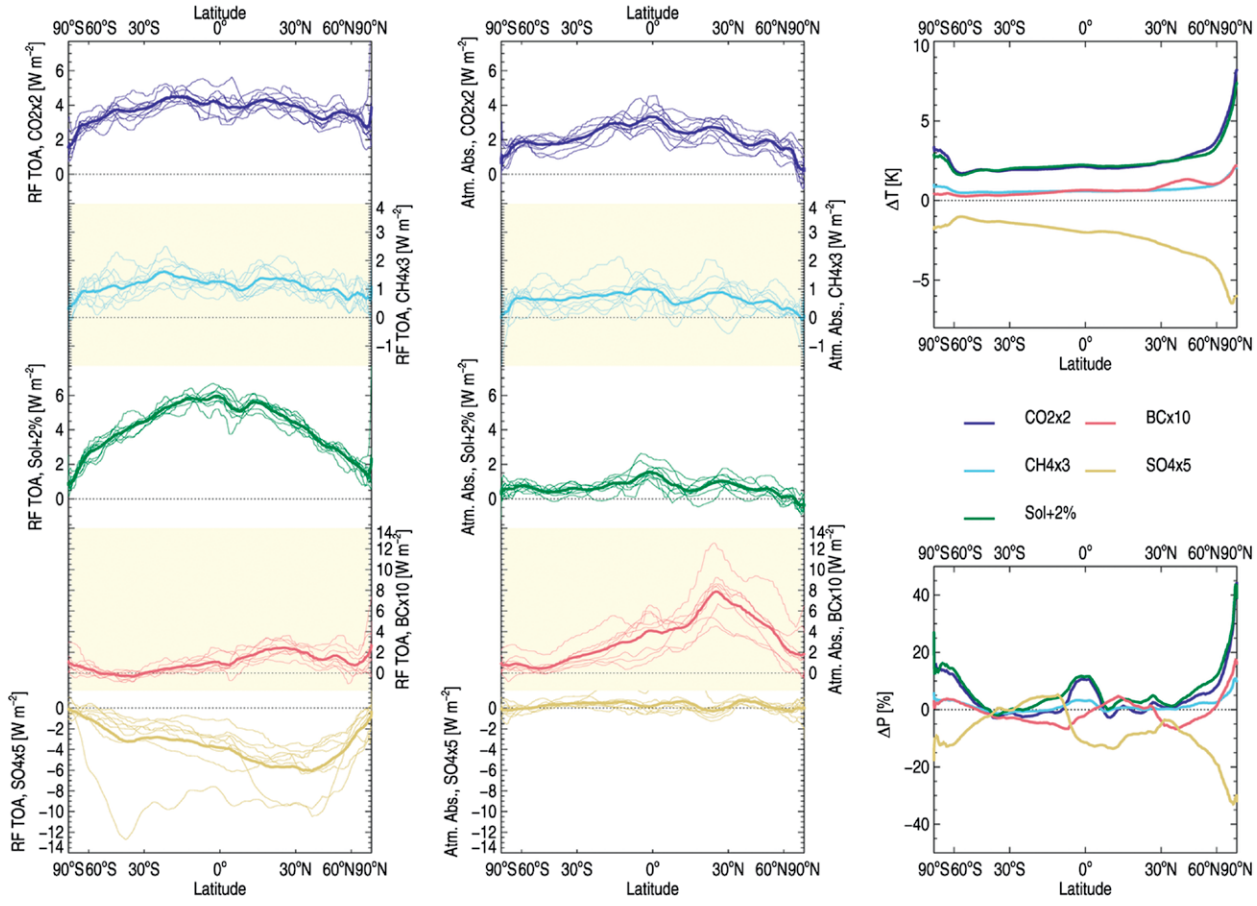

Fig. 3. Zonal- and annual-mean radiative forcing, atmospheric absorption, surface temperature change, and precipitation change for the five PDRMIP drivers. (left) The zonal annual-mean TOA radiative forcing for the five PDRMIP drivers (CO_2 in blue, CH_4 in cyan, solar in green, BC in red, and SO_4 in yellow); the individual models are shown (thin lines), in addition to the multimodel mean (thick lines). (center) As in (left), but for atmospheric absorption. (right) The (top) surface temperature and (bottom) precipitation changes for the multimodel mean for all five drivers [following the color coding from (left) and (center)]. Radiative forcing and atmospheric absorption are diagnosed from the fixed-SST simulations.

overwhelms the increase in other regions for BC on a global scale. The contrasting regional precipitation pattern is larger for BC than for the other forcing agents.

The different responses to increasing concentrations of sulfate aerosols compared to responses to solar changes illustrate that the regional pattern of the climate driver also influences the precipitation changes, with a notable shift in the ITCZ and changes across Asia. We identify stronger precipitation changes from sulfate aerosols than from greenhouse gases over Asia, similar to earlier findings (Shindell et al. 2012). Note that for an increase in sulfate aerosols the global-mean surface temperature change is negative, unlike the other climate drivers in Fig. 4. Over land, increased anthropogenic sulfate aerosols have thus generally reduced precipitation, such as over equatorial Africa or South Asia, in accordance with previous findings (Bollasina et al. 2011; Hwang et al. 2013).

Earlier studies have found that rapid adjustments have been important for global precipitation change (Andrews et al. 2010; Kvalevåg et al. 2013). Figure 4 implies that the impact of rapid adjustments on regional precipitation changes may be substantial, particularly for BC [see also Fig. 2 in Samset et al. (2016)]. Further PDRMIP studies will investigate the intermodel diversity of the hydrological sensitivity and its dependence on forcing agent and location.

Figure 5 shows changes in precipitation extremes as defined in terms of 20-yr return values of annual maximum daily precipitation, following Kharin et al. (2013). A return value for a specified N-yr return period is the value that is exceeded by an annual extreme with probability $p = 1/N$. Hence, a 20-yr return period corresponds to an annual exceedance probability of $p = 5\%$.

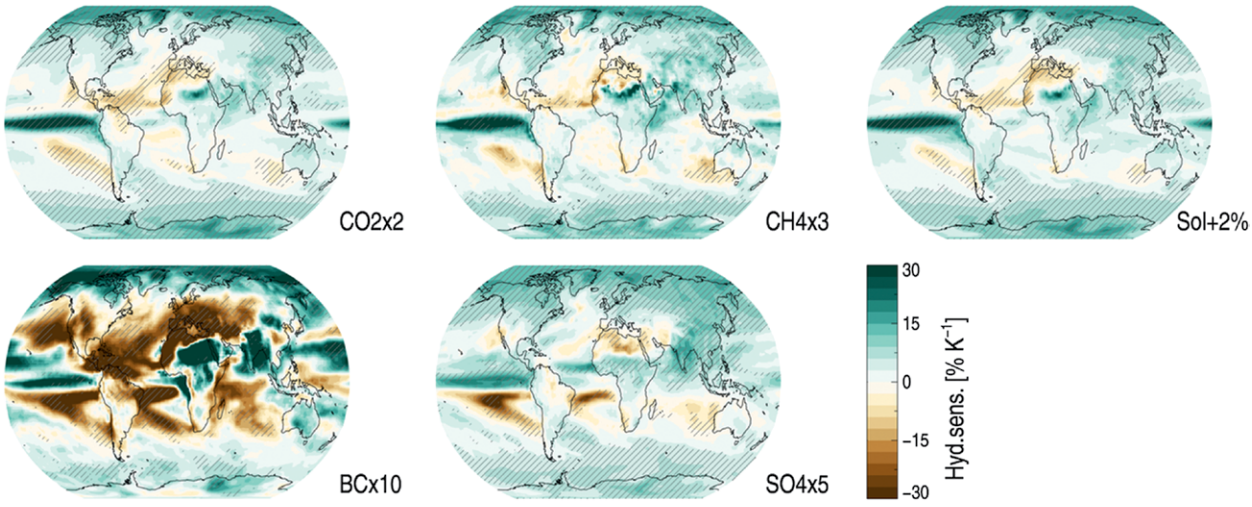

Fig. 4. Geographical distribution of the multimodel-mean apparent HS parameter for the five PDRMIP drivers experiments (CO_2 × 2, CH_4 × 3, solar + 2%, BC × 10, and SO_4 × 5). The apparent HS is calculated as the annual-mean geographical precipitation change divided by the global- and annual-mean temperature changes relative to the base simulation. The hatching is included where the mean apparent HS over the 50-yr period is more than one standard deviation away from zero.

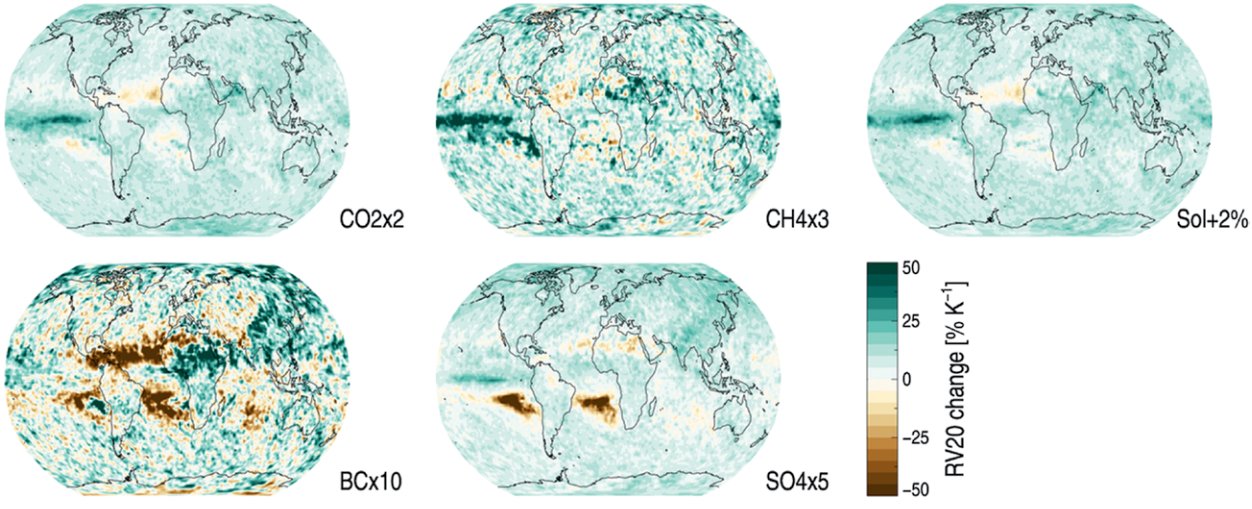

Fig. 5. Geographical distribution of multimodel-mean changes in 20-yr return values of annual maximum daily precipitation per unit of global warming for the five PDRMIP driver experiments (CO_2 × 2, CH_4 × 3, solar + 2%, BC × 10, and SO_4 × 5). The change in 20-yr return values is given as the percentage change divided by the global- and annual-mean temperature changes relative to the base simulation.

There are clear similarities between Figs. 4 and 5, but the extreme precipitation is found to increase over larger regions than the apparent HS in response to increased temperature consistent with earlier findings (Fischer et al. 2014; Pendergrass et al. 2015). For instance, regions such as the Mediterranean, which had a consistently negative HS, show increases in 20-yr return values. Part of the subtropical ocean is the only common region with a decrease in both apparent HS and the 20-yr return values. Note that the SO_4 × 5 case, unlike the other cases, gives a temperature reduction and hence a decrease in extreme precipitation.

EXPECTED OUTCOME OF PDRMIP. PDRMIP aims to enhance our scientific understanding of how individual climate drivers cause changes to mean and extreme precipitation. The PDRMIP simulations will cast light on whether different climate driver abundances are a major source of the diversity in the industrial era and future changes in precipitation among climate models by investigating the precipitation changes

and their model diversity from several individual climate drivers. Since different drivers of climate change alter the atmospheric radiation budget in different ways, it is not obvious whether changes in mean and extreme precipitation events are similar among these drivers. PDRMIP has dedicated outputs and analyses to quantify extreme precipitation and other climate extremes from the different drivers of climate change.

Two studies, each using one climate model (Andrews et al. 2010; Kvalevåg et al. 2013), have demonstrated how both the fast and slow precipitation responses depend on atmospheric absorption and surface warming, for a range of drivers of climate change. PDRMIP will quantify the generality of these findings. Energy budget calculations enhance our understanding of climate model responses (Allen and Ingram 2002; Muller and O'Gorman 2011; Kravitz et al. 2013; Hodnebrog et al. 2016; Richardson et al. 2016) and such calculations will be performed within PDRMIP in order to understand precipitation and circulation changes from the different drivers. Since we include diagnostics (top-of-the-atmosphere fluxes and surface temperature) that allow us to quantify radiative forcing in several ways (Boucher et al. 2013; Sherwood et al. 2015), PDRMIP will provide useful information on the methodology and uncertainties in radiative forcing calculations. The forcing analyses combined with energy budget analyses will provide information on the differences in climate sensitivity among the PDRMIP climate drivers and models. Shindell (2014), Rotstayn et al. (2015), and Shindell et al. (2015) found differences in the transient climate response (TCR) from inhomogeneous forcing agents. PDRMIP is a test bed for furthering our understanding of these differences in TCR.

Recent climate model simulations have shown small surface temperature responses to the current abundance of BC (Baker et al. 2015), but with relatively large intermodel variations. In PDRMIP a larger set of models will be applied with large BC perturbations and will include a number of forcing diagnostics. This will allow further analysis to better understand the finding of small surface temperature changes in Baker et al. (2015) and whether they arise from low climate sensitivity to BC or high importance of semidirect effects (Koch and Del Genio 2010; Hodnebrog et al. 2014). This analysis will be linked to possible mitigation efforts, and additional simulations with regional pollution controls applied will be investigated in terms of precipitation impacts.

SUMMARY. In PDRMIP, 10 climate modeling groups have performed common idealized simulations to enhance our understanding of the impacts of various climate drivers on precipitation. A core set of global perturbation simulations and additional regional perturbation simulations has already been performed with initial results presented in this study and in Samset et al. (2016). PDRMIP consists of step-change experiments, but this process-based approach is highly valuable for understanding current and future precipitation changes. Precipitation changes are at the heart of two of the four questions related to the World Climate Research Programme's Grand Challenge on Clouds, Circulation and Climate Sensitivity (Bony et al. 2015) and frame many of the issues considered during the Grand Challenges on Water Availability (Trenberth and Asrar 2014) and Climate Extremes. The main PDRMIP results will be analyzed during 2016–18 to feed into the next Intergovernmental Panel on Climate Change's (IPCC) Sixth Assessment Report (AR6). The main PDRMIP results will be updated online (www.cicero.uio.no/en/PDRMIP) with information on how to obtain publicly available model output. A description of available data relevant to precipitation and the energy budget are given online. Finally, descriptions of ongoing PDRMIP analyses and activities are available online and we encourage further analyses based on the PDRMIP dataset to enhance our understanding of the diverse climate driver impacts on the energy budget and precipitation.

ACKNOWLEDGMENTS. PDRMIP is partly funded through the Norwegian Research Council project NAPEX (Project 229778). TT was supported by the supercomputer system of the National Institute for Environmental Studies, Japan; the Environment Research and Technology Development Fund (S-12-3) of the Ministry of the Environment, Japan; and JSPS KAKENHI Grants 15H01728 and 15K12190. DO, AK, and TI were supported by the Norwegian Research Council through the projects EVA (Grant 229771), EarthClim (207711/E10), NOTUR (nn2345k), and NorStore (ns2345k). MK and AV are supported by the Natural Environment Research Council under Grant NE/K500872/1. Simulations with HadGEM3-GA4 were performed using the MONSooN system, a collaborative facility supplied under the Joint Weather and Climate Research Programme, which is a strategic partnership between the Met Office and the Natural Environment Research Council. TA was supported by the Joint U.K. DECC-Defra Met Office Hadley Centre Climate Programme (GA01101). We acknowledge the NASA High-End Computing Program through the NASA Center for Climate Simulation at Goddard Space Flight Center for computational resources to run the GISS-E2-R model. OB acknowledges HPC resources from CCRT under the gencmip6

allocation provided by Grand Équipement National de Calcul Intensif (GENCI). TR and PF were supported by NERC Grants NE/K007483/1 and NE/N006038/1.

REFERENCES

Allan, R. P., and B. J. Soden, 2008: Atmospheric warming and the amplification of precipitation extremes. *Science*, **321**, 1481–1484, doi:10.1126/science.1160787.

——, C. Liu, M. Zahn, D. A. Lavers, E. Koukouvagias, and A. Bodas-Salcedo, 2014: Physically consistent responses of the global atmospheric hydrological cycle in models and observations. *Surv. Geophys.*, **35**, 533–552, doi:10.1007/s10712-012-9213-z.

Allen, M. R., and W. J. Ingram, 2002: Constraints on future changes in climate and the hydrologic cycle. *Nature*, **419**, 224–232, doi:10.1038/nature01092.

Andrews, T., P. Forster, O. Boucher, N. Bellouin, and A. Jones, 2010: Precipitation, radiative forcing and global temperature change. *Geophys. Res. Lett.*, **37**, L14701, doi:10.1029/2010GL043991.

Arora, V. K., and Coauthors, 2011: Carbon emission limits required to satisfy future representative concentration pathways of greenhouse gases. *Geophys. Res. Lett.*, **38**, L05805, doi:10.1029/2010GL046270.

Baker, L. H., W. J. Collins, D. J. L. Olivié, R. Cherian, Ø. Hodnebrog, G. Myhre, and J. Quaas, 2015: Climate responses to anthropogenic emissions of short-lived climate pollutants. *Atmos. Chem. Phys.*, **15**, 8201–8216, doi:10.5194/acp-15-8201-2015.

Bala, G., K. Caldeira, and R. Nemani, 2010: Fast versus slow response in climate change: Implications for the global hydrological cycle. *Climate Dyn.*, **35**, 423–434, doi:10.1007/s00382-009-0583-y.

Ban, N., J. Schmidli, and C. Schär, 2015: Heavy precipitation in a changing climate: Does short-term summer precipitation increase faster? *Geophys. Res. Lett.*, **42**, 1165–1172, doi:10.1002/2014GL062588.

Bellouin, N., J. Rae, A. Jones, C. Johnson, J. Haywood, and O. Boucher, 2011: Aerosol forcing in the Climate Model Intercomparison Project (CMIP5) simulations by HadGEM2-ES and the role of ammonium nitrate. *J. Geophys. Res.*, **116**, D20206, doi:10.1029/2011JD016074.

Bentsen, M., and Coauthors, 2013: The Norwegian Earth System Model, NorESM1-M—Part 1: Description and basic evaluation of the physical climate. *Geosci. Model Dev.*, **6**, 687–720, doi:10.5194/gmd-6-687-2013.

Berg, P., C. Moseley, and J. O. Haerter, 2013: Strong increase in convective precipitation in response to higher temperatures. *Nat. Geosci.*, **6**, 181–185, doi:10.1038/ngeo1731.

Bollasina, M. A., Y. Ming, and V. Ramaswamy, 2011: Anthropogenic aerosols and the weakening of the South Asian summer monsoon. *Science*, **334**, 502–505, doi:10.1126/science.1204994.

Bony, S., G. Bellon, D. Klocke, S. Sherwood, S. Fermepin, and S. Denvil, 2013: Robust direct effect of carbon dioxide on tropical circulation and regional precipitation. *Nat. Geosci.*, **6**, 447–451, doi:10.1038/ngeo1799.

——, and Coauthors, 2015: Clouds, circulation and climate sensitivity. *Nat. Geosci.*, **8**, 261–268, doi:10.1038/ngeo2398.

Boucher, O., and Coauthors, 2013: Clouds and aerosols. *Climate Change 2013: The Physical Science Basis*, T. F. Stocker et al., Eds., Cambridge University Press, 571–657.

Caesar, J., and J. A. Lowe, 2012: Comparing the impacts of mitigation versus non-intervention scenarios on future temperature and precipitation extremes in the HadGEM2 climate model. *J. Geophys. Res.*, **117**, D15109, doi:10.1029/2012JD017762.

Collins, M., and Coauthors, 2013: Long-term climate change: Projections, commitments and irreversibility. *Climate Change 2013: The Physical Science Basis*, T. F. Stocker et al., Eds., Cambridge University Press, 1029–1136.

Collins, W. J., and Coauthors, 2011: Development and evaluation of an Earth-System model—HadGEM2. *Geosci. Model Dev.*, **4**, 1051–1075, doi:10.5194/gmd-4-1051-2011.

DeAngelis, A. M., X. Qu, M. D. Zelinka, and A. Hall, 2015: An observational radiative constraint on hydrologic cycle intensification. *Nature*, **528**, 249–253, doi:10.1038/nature15770.

Dong, B., R. T. Sutton, E. Highwood, and L. Wilcox, 2014: The impacts of European and Asian anthropogenic sulfur dioxide emissions on Sahel rainfall. *J. Climate*, **27**, 7000–7017, doi:10.1175/JCLI-D-13-00769.1.

Dufresne, J.-L., and Coauthors, 2013: Climate change projections using the IPSL-CM5 Earth System Model: From CMIP3 to CMIP5. *Climate Dyn.*, **40**, 2123–2165, doi:10.1007/s00382-012-1636-1.

Ferraro, A. J., and H. G. Griffiths, 2016: Quantifying the temperature-independent effect of stratospheric aerosol geoengineering on global-mean precipitation in a multi-model ensemble. *Environ. Res. Lett.*, **11**, 034012, doi:10.1088/1748-9326/11/3/034012.

Fildier, B., and W. D. Collins, 2015: Origins of climate model discrepancies in atmospheric shortwave absorption and global precipitation changes. *Geophys. Res. Lett.*, **42**, 8749–8757, doi:10.1002/2015GL065931.

Fischer, E. M., J. Sedláček, E. Hawkins, and R. Knutti, 2014: Models agree on forced response pattern of precipitation and temperature extremes. *Geophys. Res. Lett.*, **41**, 8554–8562, doi:10.1002/2014GL062018.

Fläschner, D., T. Mauritsen, and B. Stevens, 2016: Understanding the intermodel spread in global-

mean hydrological sensitivity. *J. Climate*, **29**, 801–817, doi:10.1175/JCLI-D-15-0351.1.

Flato, G., and Coauthors, 2013: Evaluation of climate models. *Climate Change 2013: The Physical Science Basis*, T. F. Stocker et al., Eds., Cambridge University Press, 741–866.

Forster, P., and Coauthors, 2007: Changes in atmospheric constituents and in radiative forcing. *Climate Change 2007: The Physical Science Basis*, S. Solomon et al., Eds., Cambridge University Press, 129–234.

Frieler, K., M. Meinshausen, T. S. von Deimling, T. Andrews, and P. Forster, 2011: Changes in global-mean precipitation in response to warming, greenhouse gas forcing and black carbon. *Geophys. Res. Lett.*, **38**, L04702, doi:10.1029/2010GL045953.

Gent, P. R., and Coauthors, 2011: The Community Climate System Model version 4. *J. Climate*, **24**, 4973–4991, doi:10.1175/2011JCLI4083.1.

Gregory, J. M., and Coauthors, 2004: A new method for diagnosing radiative forcing and climate sensitivity. *Geophys. Res. Lett.*, **31**, L03205, doi:10.1029/2003GL018747.

Hansen, J., and Coauthors, 2005: Efficacy of climate forcings. *J. Geophys. Res.*, **110,** D18104, doi:10.1029/2005JD005776.

Held, I. M., and B. J. Soden, 2006: Robust responses of the hydrological cycle to global warming. *J. Climate*, **19**, 5686–5699, doi:10.1175/JCLI3990.1.

Hodnebrog, Ø., G. Myhre, and B. H. Samset, 2014: How shorter black carbon lifetime alters its climate effect. *Nat. Commun.*, **5**, 5065, doi:10.1038/ncomms6065.

——, ——, P. M. Forster, J. Sillmann, and B. H. Samset, 2016: Local biomass burning is a dominant cause of the observed precipitation reduction in southern Africa. *Nat. Commun.*, **7**, 11236, doi:10.1038/ncomms11236.

Hurrell, J. W., and Coauthors, 2013: The Community Earth System Model: A framework for collaborative research. *Bull. Amer. Meteor. Soc.*, **94**, 1339–1360, doi:10.1175/BAMS-D-12-00121.1.

Hwang, Y.-T., D. M. W. Frierson, and S. M. Kang, 2013: Anthropogenic sulfate aerosol and the southward shift of tropical precipitation in the late 20th century. *Geophys. Res. Lett.*, **40**, 2845–2850, doi:10.1002/grl.50502.

IPCC, 2013: Summary for policymakers. *Climate Change 2013: The Physical Science Basis*, T. F. Stocker et al., Eds., Cambridge University Press, 1–29.

Iversen, T., and Coauthors, 2013: The Norwegian Earth System Model, NorESM1-M—Part 2: Climate response and scenario projections. *Geosci. Model Dev.*, **6**, 389–415, doi:10.5194/gmd-6-389-2013.

Kay, J. E., and Coauthors, 2015: The Community Earth System Model (CESM) large ensemble project: A community resource for studying climate change in the presence of internal climate variability. *Bull. Amer. Meteor. Soc.*, **96**, 1333–1349, doi:10.1175/BAMS-D-13-00255.1.

Kendon, E. J., N. M. Roberts, H. J. Fowler, M. J. Roberts, S. C. Chan, and C. A. Senior, 2014: Heavier summer downpours with climate change revealed by weather forecast resolution model. *Nat. Climate Change*, **4**, 570–576, doi:10.1038/nclimate2258.

Kharin, V. V., F. W. Zwiers, X. Zhang, and M. Wehner, 2013: Changes in temperature and precipitation extremes in the CMIP5 ensemble. *Climatic Change*, **119**, 345–357, doi:10.1007/s10584-013-0705-8.

Kirkevåg, A., and Coauthors, 2013: Aerosol–climate interactions in the Norwegian Earth System Model-NorESM1-M. *Geosci. Model Dev.*, **6**, 207–244, doi:10.5194/gmd-6-207-2013.

Knutti, R., and J. Sedláček, 2013: Robustness and uncertainties in the new CMIP5 climate model projections. *Nat. Climate Change*, **3**, 369–373, doi:10.1038/nclimate1716.

——, D. Masson, and A. Gettelman, 2013: Climate model genealogy: Generation CMIP5 and how we got there. *Geophys. Res. Lett.*, **40**, 1194–1199, doi:10.1002/grl.50256.

Koch, D., and A. D. Del Genio, 2010: Black carbon semi-direct effects on cloud cover: Review and synthesis. *Atmos. Chem. Phys.*, **10**, 7685–7696, doi:10.5194/acp-10-7685-2010.

Kravitz, B., and Coauthors, 2013: An energetic perspective on hydrological cycle changes in the Geoengineering Model Intercomparison Project. *J. Geophys. Res. Atmos.*, **118**, 13 087–13 102, doi:10.1002/2013JD020502.

Kvalevåg, M. M., B. H. Samset, and G. Myhre, 2013: Hydrological sensitivity to greenhouse gases and aerosols in a global climate model. *Geophys. Res. Lett.*, **40**, 1432–1438, doi:10.1002/grl.50318.

Lenderink, G., and E. Van Meijgaard, 2008: Increase in hourly precipitation extremes beyond expectations from temperature changes. *Nat. Geosci.*, **1**, 511–514, doi:10.1038/ngeo262.

MacIntosh, C. R., R. P. Allan, L. H. Baker, N. Bellouin, W. Collins, Z. Mousavi, and K. P. Shine, 2016: Contrasting fast precipitation responses to tropospheric and stratospheric ozone forcing. *Geophys. Res. Lett.*, **43**, 1263–1271, doi:10.1002/2015GL067231.

Martin, G. M., and Coauthors, 2011: The HadGEM2 family of Met Office Unified Model climate configurations. *Geosci. Model Dev.*, **4**, 723–757, doi:10.5194/gmd-4-723-2011.

Mehran, A., A. AghaKouchak, and T. J. Phillips, 2014: Evaluation of CMIP5 continental precipitation

simulations relative to satellite-based gauge-adjusted observations. *J. Geophys. Res. Atmos.*, **119**, 1695–1707, doi:10.1002/2013JD021152.

Merlis, T. M., 2015: Direct weakening of tropical circulations from masked CO_2 radiative forcing. *Proc. Natl. Acad. Sci. USA*, **112**, 13 167–13 171, doi:10.1073/pnas.1508268112.

Ming, Y., V. Ramaswamy, and G. Persad, 2010: Two opposing effects of absorbing aerosols on global-mean precipitation. *Geophys. Res. Lett.*, **37**, L13701, doi:10.1029/2010GL042895.

Mitchell, J. F. B., C. A. Wilson, and W. M. Cunnington, 1987: On CO_2 climate sensitivity and model dependence of results. *Quart. J. Roy. Meteor. Soc.*, **113**, 293–322, doi:10.1256/smsqj.47516.

Muller, C. J., and P. A. O'Gorman, 2011: An energetic perspective on the regional response of precipitation to climate change. *Nat. Climate Change*, **1**, 266–271, doi:10.1038/nclimate1169.

Myhre, G., and Coauthors, 2013a: Anthropogenic and Natural Radiative Forcing. *Climate Change 2013: The Physical Science Basis*, T. F. Stocker et al., Eds., Cambridge University Press, 659–740.

——, and Coauthors, 2013b: Radiative forcing of the direct aerosol effect from AeroCom Phase II simulations. *Atmos. Chem. Phys.*, **13**, 1853–1877, doi:10.5194/acp-13-1853-2013.

Neale, R. B., and Coauthors, 2010: Description of the NCAR Community Atmosphere Model (CAM 4.0). NCAR Tech. Rep. NCAR/TN-485+STR, 212 pp. [Available online at www.cesm.ucar.edu/models/ccsm4.0/cam/docs/description/cam4_desc.pdf.]

O'Gorman, P. A., 2015: Precipitation extremes under climate change. *Curr. Climate Change Rep.*, **1**, 49–59, doi:10.1007/s40641-015-0009-3.

——, R. P. Allan, M. P. Byrne, and M. Previdi, 2012: Energetic constraints on precipitation under climate change. *Surv. Geophys.*, **33**, 585–608, doi:10.1007/s10712-011-9159-6.

Otto-Bliesner, B. L., and Coauthors, 2016: Climate variability and change since 850 CE: An ensemble approach with the Community Earth System Model. *Bull. Amer. Meteor. Soc.*, **97**, 735–754, doi:10.1175/BAMS-D-14-00233.1.

Pendergrass, A. G., and D. L. Hartmann, 2012: Global-mean precipitation and black carbon in AR4 simulations. *Geophys. Res. Lett.*, **39**, L01703, doi:10.1029/2011GL050067.

——, and ——, 2014: The atmospheric energy constraint on global-mean precipitation change. *J. Climate*, **27**, 757–768, doi:10.1175/JCLI-D-13-00163.1.

——, F. Lehner, B. M. Sanderson, and Y. Xu, 2015: Does extreme precipitation intensity depend on the emissions scenario? *Geophys. Res. Lett.*, **42**, 8767–8774, doi:10.1002/2015GL065854.

Previdi, M., 2010: Radiative feedbacks on global precipitation. *Environ. Res. Lett.*, **5**, 025211, doi:10.1088/1748-9326/5/2/025211.

Richardson, T. B., P. M. Forster, T. Andrews, and D. J. Parker, 2016: Understanding the rapid precipitation response to CO_2 and aerosol forcing on a regional scale. *J. Climate*, **29**, 583–594, doi:10.1175/JCLI-D-15-0174.1.

Rotstayn, L. D., M. A. Collier, D. T. Shindell, and O. Boucher, 2015: Why does aerosol forcing control historical global-mean surface temperature change in CMIP5 models? *J. Climate*, **28**, 6608–6625, doi:10.1175/JCLI-D-14-00712.1.

Samset, B. H., and Coauthors, 2016: Fast and slow precipitation responses to individual climate forcers: A PDRMIP multimodel study. *Geophys. Res. Lett.*, **43**, 2782–2791, doi:10.1002/2016GL068064.

Schmidt, G. A., and Coauthors, 2014: Configuration and assessment of the GISS ModelE2 contributions to the CMIP5 archive. *J. Adv. Model. Earth Syst.*, **6**, 141–184, doi:10.1002/2013MS000265.

Shaw, T. A., and A. Voigt, 2015: Tug of war on summertime circulation between radiative forcing and sea surface warming. *Nat. Geosci.*, **8**, 560–566, doi:10.1038/ngeo2449.

Sherwood, S. C., S. Bony, O. Boucher, C. Bretherton, P. M. Forster, J. M. Gregory, and B. Stevens, 2015: Adjustments in the forcing-feedback framework for understanding climate change. *Bull. Amer. Meteor. Soc.*, **96**, 217–228, doi:10.1175/BAMS-D-13-00167.1.

Shindell, D. T., 2014: Inhomogeneous forcing and transient climate sensitivity. *Nat. Climate Change*, **4**, 274–277, doi:10.1038/nclimate2136.

——, A. Voulgarakis, G. Faluvegi, and G. Milly, 2012: Precipitation response to regional radiative forcing. *Atmos. Chem. Phys.*, **12**, 6969–6982, doi:10.5194/acp-12-6969-2012.

——, G. Faluvegi, L. Rotstayn, and G. Milly, 2015: Spatial patterns of radiative forcing and surface temperature response. *J. Geophys. Res. Atmos.*, **120**, 5385–5403, doi:10.1002/2014JD022752.

Sillmann, J., V. V. Kharin, F. W. Zwiers, X. Zhang, and D. Bronaugh, 2013a: Climate extremes indices in the CMIP5 multimodel ensemble: Part 2. Future climate projections. *J. Geophys. Res. Atmos.*, **118**, 2473–2493, doi:10.1002/jgrd.50188.

——, L. Pozzoli, E. Vignati, S. Kloster, and J. Feichter, 2013b: Aerosol effect on climate extremes in Europe under different future scenarios. *Geophys. Res. Lett.*, **40**, 2290–2295, doi:10.1002/grl.50459.

Stephens, G. L., and Coauthors, 2012: An update on Earth's energy balance in light of the latest global

observations. *Nat. Geosci.*, **5**, 691–696, doi:10.1038/ngeo1580.

Stier, P., and Coauthors, 2013: Host model uncertainties in aerosol radiative forcing estimates: Results from the AeroCom Prescribed Intercomparison Study. *Atmos. Chem. Phys.*, **13**, 3245–3270, doi:10.5194/acp-13-3245-2013.

Takahashi, K., 2009: The global hydrological cycle and atmospheric shortwave absorption in climate models under CO_2 forcing. *J. Climate*, **22**, 5667–5675, doi:10.1175/2009JCLI2674.1.

Takemura, T., T. Nozawa, S. Emori, T. Y. Nakajima, and T. Nakajima, 2005: Simulation of climate response to aerosol direct and indirect effects with aerosol transport-radiation model. *J. Geophys. Res.*, **110**, D02202, doi:10.1029/2004jd005029.

——, M. Egashira, K. Matsuzawa, H. Ichijo, R. O'Ishi, and A. Abe-Ouchi, 2009: A simulation of the global distribution and radiative forcing of soil dust aerosols at the Last Glacial Maximum. *Atmos. Chem. Phys.*, **9**, 3061–3073, doi:10.5194/acp-9-3061-2009.

Trenberth, K. E., 2011: Changes in precipitation with climate change. *Climate Res.*, **47**, 123–138, doi:10.3354/cr00953.

——, and G. R. Asrar, 2014: Challenges and opportunities in water cycle research: WCRP contributions. *Surv. Geophys.*, **35**, 515–532, doi:10.1007/s10712-012-9214-y.

Walters, D. N., and Coauthors, 2014: The Met Office Unified Model Global Atmosphere 4.0 and JULES Global Land 4.0 configurations. *Geosci. Model Dev.*, **7**, 361–386, doi:10.5194/gmd-7-361-2014.

Wasko, C., A. Sharma, and S. Westra, 2016: Reduced spatial extent of extreme storms at higher temperatures. *Geophys. Res. Lett.*, **43**, 4026–4032, doi:10.1002/2016GL068509.

Watanabe, M., and Coauthors, 2010: Improved climate simulation by MIROC5: Mean states, variability, and climate sensitivity. *J. Climate*, **23**, 6312–6335, doi:10.1175/2010JCLI3679.1.

Westra, S., L. V. Alexander, and F. W. Zwiers, 2013: Global increasing trends in annual maximum daily precipitation. *J. Climate*, **26**, 3904–3918, doi:10.1175/JCLI-D-12-00502.1.

——, and Coauthors, 2014: Future changes to the intensity and frequency of short-duration extreme rainfall. *Rev. Geophys.*, **52**, 522–555, doi:10.1002/2014RG000464.

Yoshimori, M., and A. J. Broccoli, 2008: Equilibrium response of an atmosphere–mixed layer ocean model to different radiative forcing agents: Global and zonal mean response. *J. Climate*, **21**, 4399–4423, doi:10.1175/2008JCLI2172.1.